7. Experimental identification of non-linear and hysteretic models for masonry structures

This chapter describes the results of experimental testing campaigns performed on a masonry twin-arch bridge model. This research has been conducted within the experimental activities of the Earthquake Engineering & Dynamics Lab at the Politecnico di Torino. A scaled physical model has been built in order to study the effect of the central pile settlement due to riverbank erosion. The two-span masonry bridge model underwent different damage levels caused by the differential settlements applied to the central pier. For each settlement step, harmonic shaker tests were conducted under different excitation levels, this allowing for non-linear identification of the progressively damaged system. In a first stage, non-linearity has been detected by relying to classical linearization concepts. Then, non-linear identification methods working in the time-frequency domain, as those proposed in Chapter 6, have been applied to shaker test data, in order to estimate non-linear and hysteretic parameters. The identified model, which is suited for masonry under dynamic loading, can corroborate 3D numerical models for using in the reassessment of existing structures.

7.1 Scaled model of a masonry twin-arch bridge

The 1:2 scaled model of the masonry arch bridge shown in figure 7.1 was built in the laboratory of the Department of Structural, Geotechnical and Building Engineering at the Politecnico di Torino. The prototype this model comes from is not a real existing bridge but was designed taking the masonry arch bridges common features, geometric proportions and historical design codes into account [1,2].

The model is a twin-arch bridge with a length of 5.90 m, a width of 1.60 m and it is 1.75 m high. The two arches are segmental arches with a radius of 2.00 m and an angular opening of 30°. Each span is 2.00 m long between the supports and the thickness of the arch is equal to 0.20m. The model was built with handmade clay bricks also scaled to 130x65x30 mm to respect the adopted modelling scale law. Low compressive strength elements were chosen and a mortar with poor mechanical properties was used to bound them in order to reproduce the typical materials of historical constructions.

Figure 7.1 - The scaled masonry bridge: notice the settlement application device under the central pier.

The mid-span masonry pier, which was cut at a hypothetical middle-height section to allow the insertion of a settlement application system, is imagined to be placed inside the streambed and subjected to the scour of its foundation.

Some hydraulic flume tests were carried out on a further scaled down model of the bridge pier in order to simulate the scour effects in the lab. The foundation settlements and rotations resulting from these investigations were then replicated on the bridge model by means of the four independent screws installed at the extremities of the settlement application system. The spherical plain bearings placed at the head of the screws allow the rotations of the plate which support the central pier about axes parallel to the longitudinal and transversal directions of the bridge.

In order to simulate the streambed material surrounding the foundation of the central pier, a polystyrene mould was introduced. In this way a polystyrene layer interfaces the pier and the settlement application device and a polystyrene ring surrounds the pier.

The experimental investigations carried out on the masonry arch bridge model were divided in two different sessions. In the first session most of the efforts were addressed to reduce the high uncertainties referred to the material properties and the structural behaviour of this complex structure. Several destructive tests were performed on samples collected during the model construction in order to estimate the mechanical properties of the masonry material. The estimated parameters were then introduced in a numerical model of the bridge to obtain a preliminary calculation of the modal parameters. The information acquired in these initial analyses was helpful to plan the following dynamic tests and to interpret the first results of the modal identification. In this phase also hydraulic tests on a reduced model of the central pier were carried out in order to quantify the settlement to be applied.

7.1.1 Material characterisation tests

Several tests were carried out in order to characterise the mechanical properties of the mortar and of the masonry used to build model (for further information see Ruocci [1]).

The characterisations tests on the mortar samples were performed following the prescriptions proposed by the European standard code EN 998-2:2003 adapted to take in account the scaled measure of bricks. The collected samples belong to the M2.5 class of the European standard code EN 998-2:2003 which is one of the poorest in terms of mechanical properties.

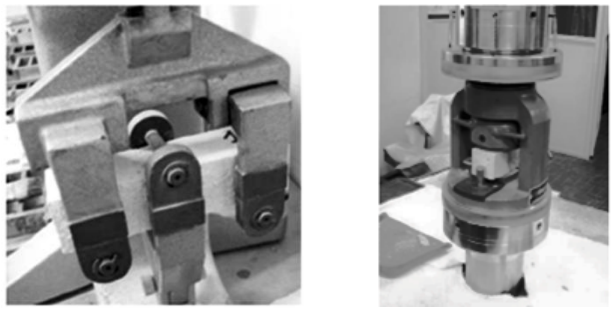

Figure 7.2 - Tests carried out on mortar samples.

The characterisations tests on the masonry samples were performed following the prescriptions proposed by the European standard code UNI EN 1052-1, EN 1052-3:2002 and the American standard code ASTM E 518-02. The masonry samples were adapted in order to resemble the shape of required test specimens while the testing procedures were followed strictly. The destructive tests performed on the masonry samples were:

- axial compression on cubic samples;
- diagonal compression on cubic samples;
- shear test on masonry triplets;
- four points bending test on a segment of arch.

Figure 7.3 - Tests conducted on the masonry samples.

Test	μ [N/mm2]	σ [N/mm2]
Compressive tests: tensile strength	4.278	0.354
Compressive tests: Young modulus E	1451	472
Diagonal tests: tensile strength	0.304	0.088
Diagonal tests: shear strength	0.430	0.125
Diagonal tests: shear Young modulus G	940	436
Shear tests (0.1 kN pre-compression): shear strength	0.794	0.301
Shear tests (0.5 kN pre-compression): shear strength	1.013	0.188
Four points bending tests: R modulus of rupture	0.22	//

Table 7.1 - Results from the compressive tests, diagonal tests, shear tests and four point bending tests.

7.1.2 Flume tests

The hydraulic model was designed scaling the pier dimensions down so that the ratio between the length of the bridge and the width of the pier was maintained. The bottom section of the pier scaled model was connected with a hypothetic foundation base. The rectangular foundation was dipped into the bed material, whose uniform mean diameter was 0.80 mm, while the pier was hung up but not allowed to move during the flume tests.

The evolution of the soil profile produced by the induced scour was periodically monitored through a laser scanner acquired by a digital camera. The images taken during the tests were then automatically processed to define the portion of the foundation lateral face not covered by the bed material at each time step. The corresponding portion on the arch bridge model was freed from the polystyrene ring surrounding the bottom part of the pier to simulate the reduction of the lateral restrain at the foundation base.

Also the undermining effects were experienced in the flume tests, especially when the foundation base was not excessively dipped in the bed material. The erosion of the soil underneath the foundation, and consequently the loss of its bearing action, is simulated in the experimental model through the settlements application device previously described.

7.1.3 Numerical models

A 3D numerical model of the arch bridge was realised in the ADINA Finite Element package to estimate and assimilate modal parameters. The purpose was to better understand the dynamic behaviour of the structure and to plan accurately the following vibration analyses. In fact, the selection of the sensors location must be assessed carefully in order to allow a suitable resolution in the mode shapes for the highest number of identified modes.

The model consists mainly in solid elements and spring elements able to simulate the polystyrene layer and the settlement application device. The mechanical properties have been inherited from the material characterisation tests. The model is subdivided into a series of elements groups, where each group includes all those finite elements which share common mechanical features or structural functions.

In order to predict cracks locations, a numerical model of the masonry arch bridge [1] was built in the DIANA FE package which was able to simulate the non-linear behaviour of masonry. The FE package implemented a smeared cracking model which

incorporates a tension cut-off, tension softening and shear retention. After the results of non-linear analysis, it was decided to add masses at the top of the central pier so as to take in account the weight of the missing part of the pier and to partially compensate the arch effect developed by massive abutments.

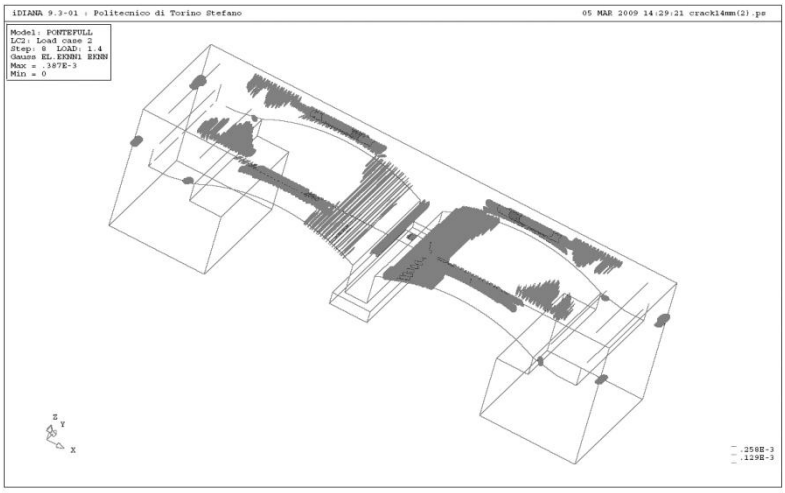

Figure 7.4 - Non-linear model: smeared crack pattern with an applied settlement of 14 mm.

7.2 Dynamic experimental tests

7.2.1 Experimental test program

As previously stated, the main objective of the experimental test was to determine the capability of a structural health monitoring system, based mainly on dynamic measures, to detect the occurring of damage (such as scour at the bridge pier foundation). In this framework, dynamic testing ensures to identify a set of parameters to be monitored. A sensitivity analysis has been carried out on the parameters to choose the most reliable to detect the damage.

Several damage steps have been applied to the structure in accordance with hydraulic flume tests as shown in Table 7.2.

Experimental campaign	Damage steps	Settlement [mm]	Rotation [rad]	Polystyrene
1st campaign	Healthy State (HS)	0	0	0%
2nd campaign	DS1	0	0	18%
	DS2	0.25	0	25%
	DS3	1	4.21E-04	37.5%
	DS4	2.25	1.01E-03	47%
3rd campaign	DS5	2.25	1.23E-03	56%
	DS6	2.8	1.23E-03	72%
	DS7	3.6	1.27E-03	81%
	DS8	4.7	1.30E-03	91%
	DS9	7.6	1.28E-03	100%

Table 7.2 - Damage steps, middle pier settlement, pier rotation, polystyrene removed.

	Time	Step	Excitation	Measurements
1st campaign	October 2008	HS	AV, IH	ACC, SG, T, OPT
	November 2008	HS	AV, IH	ACC, SG, T, OPT
	January 2009	HS	AV, IH	ACC, SG, T, OPT
	February 2009	HS	AV, IH	ACC, SG, T, OPT
	March 2009	HS	AV, IH	ACC, SG, T, OPT
2nd campaign	April 2009	HS (applied masses)	AV, IH	ACC, SG, T, OPT
		DS1	AV, IH, S	ACC, SG, T, OPT
		DS2	AV, IH, S	ACC, SG, T, OPT
		DS3	AV, IH, S	ACC, SG, T, OPT
		DS4	AV, IH, S	ACC, SG, T, OPT
3rd campaign	September 2010	HS (post-relaxation)	AV, IH, S	ACC, SG, T, OPT
		DS5	AV, IH, S	ACC, SG, T, OPT
	October 2010	DS6	AV, IH, S	ACC, SG, T, OPT
		DS7	AV, IH, S	ACC, SG, T, OPT
		DS8	AV, IH, S	ACC, SG, T, OPT
		DS9	AV, IH, S	ACC, SG, T, OPT

Table 7.3 - Experimental tests timeline.

Table 7.3 shows the timeline of the experimental tests. Different excitation sources were applied to the bridge model: ambient vibrations (AV), impact hammer (IH) and a shaker (S). Several physical quantities were monitored under the different excitations: acceleration measurements (ACC), strain deformation (SG and OPT) and temperature (T).

The experimental test involved three different experimental campaigns. The first campaign regarded the undamaged structure (October 2008 - March 2009): an extensive set of dynamic tests was carried out on the bridge model in order to characterise its "healthy" state (HS). Monitoring of dynamical properties of the bridge showed a decrease in the structure stiffness through the whole campaign. This may be due to the development of some rheologic phenomena, like the concrete blocks creep or the mortar shrinkage, leading to strains incompatible with the stiffness of the arch barrels, might have produced a partial detachment between the masonry abutments and the arch barrels.

The second campaign (April 2009) started after the application of additional masses on the central pier, in order to take in account the weight of the missing part of

the pier. In the same campaign the first four settlement steps were applied on the upstream side of the pier. In addition, parts of the polystyrene ring were removed at each step to simulate the erosion of streambed around the foundation accordingly to hydraulic flume tests. Dynamical tests were conducted in correspondence of each settlement step.

During the latter campaign (September 2010 - October 2010) five further settlement steps were applied. In this phase the removal of the polystyrene ring continued until all the polystyrene was removed.

7.2.2 Experimental setups

Dynamical vibration tests require a careful identification of an optimal sensor location. In order to achieve a good mode shapes resolution, a heuristic approach was employed. The arch barrels were subdivided in 11 segments whose ends were assumed as measuring points for both the edge and the middle lines. Other 6 positions at the springing sections of the pier were materialised to capture the longitudinal displacements. The 4 mid-span sections of the arch barrels lateral faces and the 2 pier frontal faces were considered for the lateral and torsional modes. Finally, the 2 positions on the longitudinal spandrel walls at the middle section of the deck were added to identify the vertical modes.

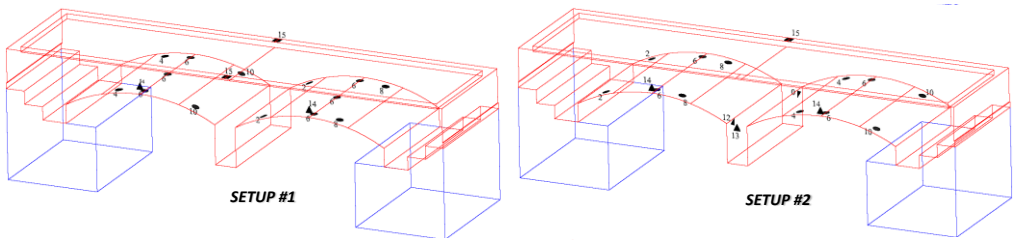

Figure 7.5 - Experimental setups for vibration tests.

The sampling frequency was fixed to a value of 400 Hz to acquire the signals produced by both ambient noise and impact hammer excitations, using an instrumented hammer. A 180 seconds time laps was adopted for the ambient noise acquisitions. Several impacts were acquired in a 60 seconds time, even if only one impact per acquisition was used in the dynamic identification. The hammer impacts were applied in the same sensors positions along the longitudinal, transversal and vertical directions of the bridge model in order to excite properly all the modes estimated by the numerical modal analysis. Two setups were used for each vibration tests in order to capture the higher number of natural modes. Each setup consisted of 18 channels leading to 36 instrumented positions.

Forced vibration tests were performed by using a shaker TIRA TV 51220, capable to supply a rated peak force of 200 N. The force applied was acquired by using a mechanical impedance sensor PCB Piezotronics 288D01 (measurement range ±222.4 N pk). Five type of excitation tests were carried out:

- random: random excitation in a 10-100 Hz band,

- sweep sine: linear chirp from 10 to 100 Hz,
- shock: impulsive excitation,
- resonance: sine excitation at resonance frequencies,
- sine: sine excitation from 10 to 100 Hz, with 1 Hz resolution.

7.2.3 Accelerometers

The selected sensors for the dynamic tests performed on the structure were capacitive accelerometers. The employed dynamic acquisition system was composed by a set of 18 monoaxial PCB Piezotronics accelerometers with a sensitivity of 1V/g, a measurement range of ±3g, a broadband resolution of 30 μg and a weight of 17.5g. The accelerometers were connected through coaxial cables to the LMS Difa-Scadas data acquisition system which provided also the signals amplification. The acquired signals were recorded on the hard drive of a laptop computer interfaced with the data acquisition system and running a specific signal acquisition software.

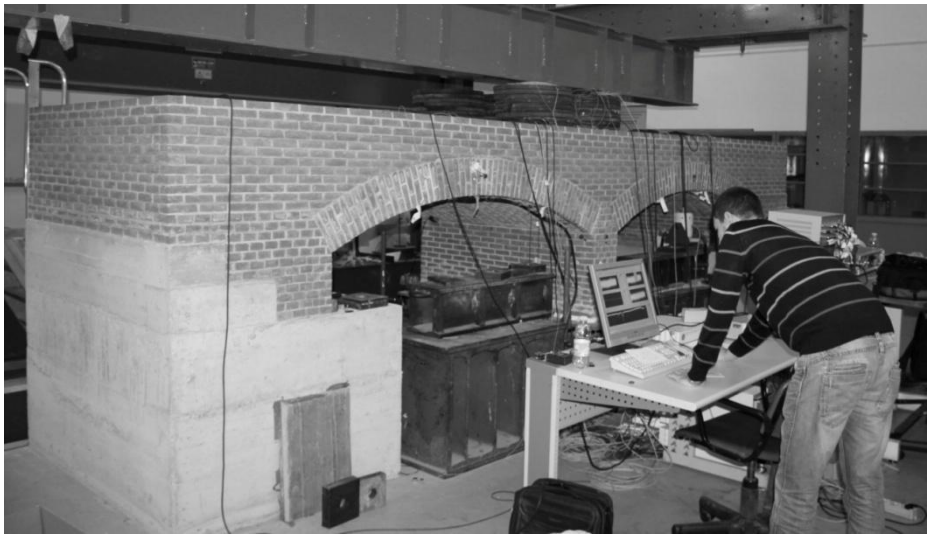

Figure 7.6 - Accelerometers setup with acquisition system.

7.2.4 Strain gauges

The responses of the arch barrels to the settlements application were measured by means of a set of 16 120 Ω resistive strain gages 160mm long and 10mm wide. The length of the strain gages allowed to cross at least five bricks and thus to obtain a representative information of the masonry behaviour. The transducers were divided into two sets and were uniformly distributed on the intrados of the arch barrels at the upstream side of the bridge model. As expected from the numerical analyses, the settlement application led to tensile strains in the central portion of the bridge and

compressions in the lateral parts. The distribution of the strains throughout the first three steps resulted unchanged and a progressive increase of the deformations was recorded.

7.2.5 Visually detectable damage

Figure 7.7 shows the crack patterns visually detectable on the arch barrels and at the interface between the arches and the spandrel walls after the last settlements application. It is worthy to emphasise an important point related to the visual detection of the cracks openings. Damage was not observed immediately after the settlement step application but within the lapse of time between two successive steps. This aspect can be reasonably ascribed to a continuous evolution of the pier settlement effects in time. Several papers on damage detection of this object have been published [1,3,4].

Figure 7.7 - Damage in the bridge after the third testing campaign.

7.3 Identification campaign

7.3.1 Data analysis and assimilation

The first step of the data analysis consisted of an experimental modal analysis. It was decided to employ two techniques working in the time domain due to the great spectral resolution they offer and their modal uncoupling capability. The Eigenvalue Realization Algorithm (ERA) was used to analyse the free decay responses, whilst ambient vibration signals called for a Stochastic Subspace Identification (SSI).

7.3.1.1 Modal parameters and symptoms evolution

The estimation of both natural frequencies and damping did not show a monotonic trend during the different campaigns. Figure 7.8 shows the trend of the first four natural frequencies and dampings. It is noteworthy that, whilst in second campaign the trend of the first frequency is almost monotonic and highlights stiffness degradation (mainly related to the boundary conditions of the pier); in the third campaign the

interpretation of the curve is more complex. Firstly, the first frequency increased up to 19.23 Hz, this meaning that relaxation made pier settle, increasing the boundary condition stiffness. In fact, after DS 4, the pier was almost completely suspended. Secondly, this phenomenon governs mainly the first modal shape, as it can be seen from 2nd and 4th natural frequencies which retain their values almost equal between the 2nd and the 3rd campaign.

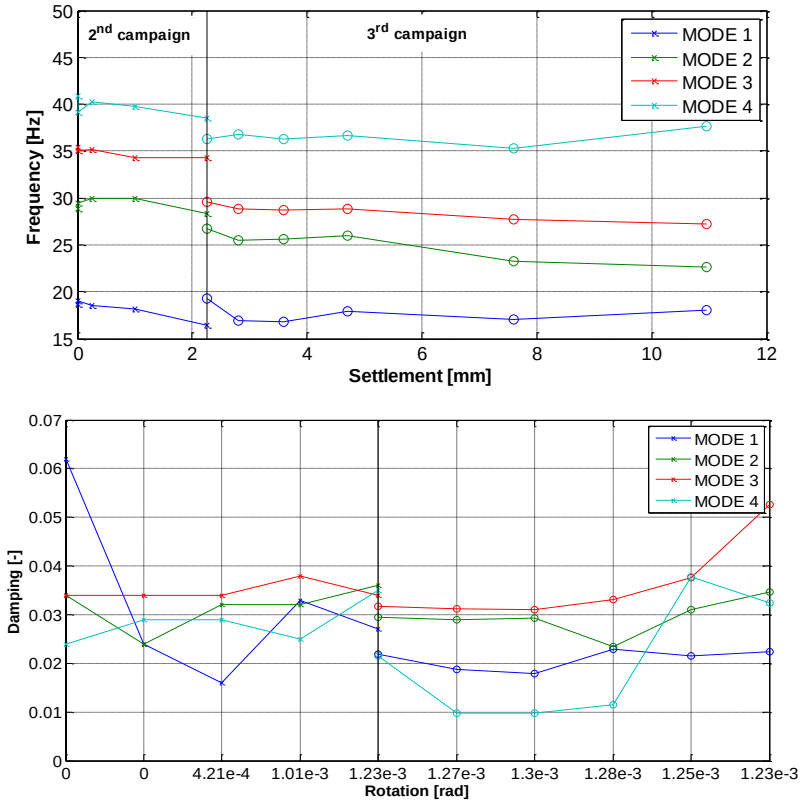

Figure 7.8 - Natural frequencies and dampings of the first 4 modes through the various damage steps (damage step 0 corresponds to the healthy state of the bridge). Left side: 2nd campaign. Right side: 3rd campaign.

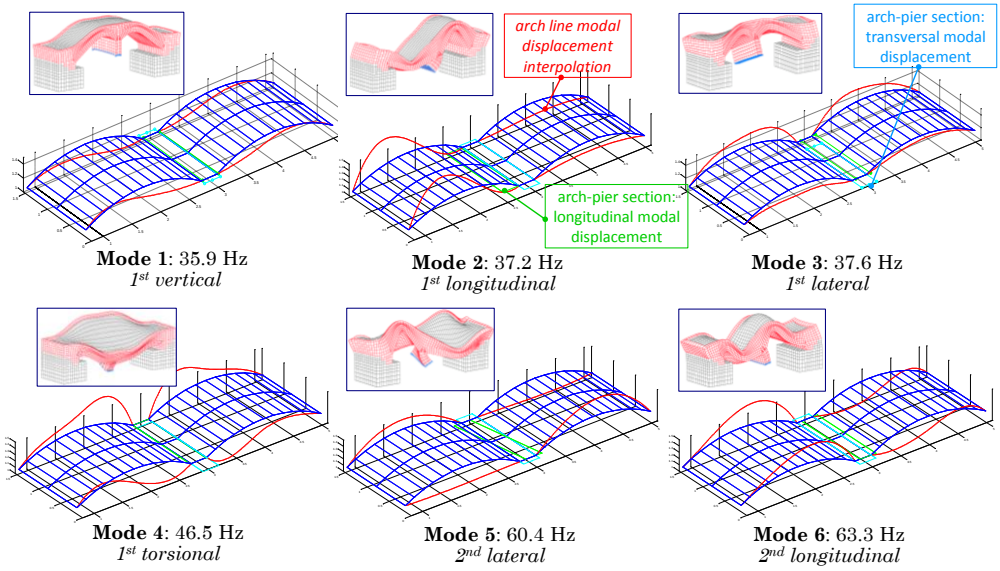

Figure 7.9 - Experimental and numerical modal shapes (Frequency values related to the not updated FE model).

7.3.2 *Study of the transient after the application of settlements*

Diagrams such as those represented in figure 7.8 pose important problems about the real capacity of current diagnostic tools to distinguish between changes in linear parameters induced by damage and other rheologic and indirect actions, including relaxation, ageing etc. In order to derive information about the evolution of the modal parameters throughout the settlements application, the dynamic response was represented in the time-frequency domain by the Choi-Williams transform [5]. A non-stationary behaviour was detected relatively to highly coupled modes in the high frequencies range.

In order to further investigate the transient phenomena, an instantaneous estimation of the modal parameters associated with the Frequency Response Function (FRF), was carried out. The implemented methodology follows the optimisation procedure proposed by Ceravolo in [6].

Figure 7.10 shows the results of the curve fitting procedure used to calibrate the modal parameters estimates. This allowed detecting the decreasing and increasing variation of the natural frequency and the damping ratio of the first identified mode, respectively. The increase in relative damping here is fictitious, being associated to the assumption of viscous damping.

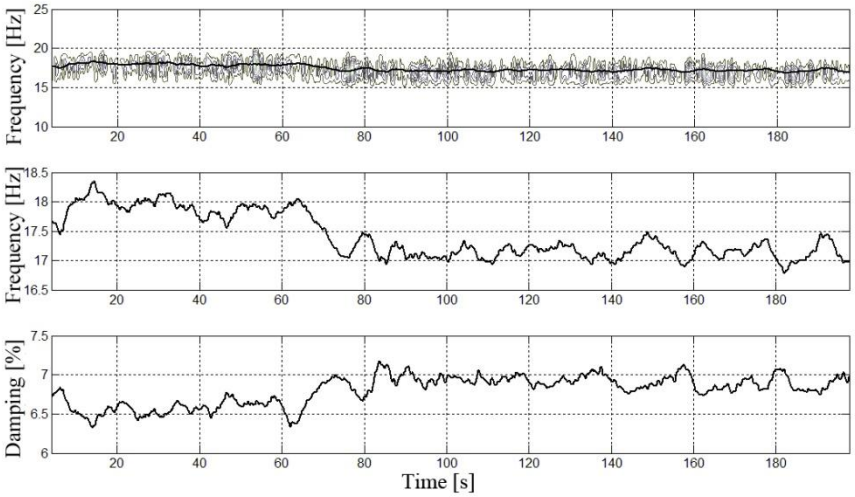

Figure 7.10. Results of the curve-fitting procedure for the first vibration mode: Spectrogram of a filtered signal (top), modal frequency istantaneous estimate (middle), damping istantaneous estimate (bottom).

7.4 Dynamic monitoring of the parameters at different damage levels

7.4.1 Non-linear identification in principal coordinates

Classical linear theory allows the decoupling of motion equation in terms of modal or principal coordinates. On the other hand, several authors investigated the non-linear vibration of mechanical systems also in the principal coordinates - for instance see Bellizzi & Bouc [7] or Spottswood & Allemang [8] - though in such a case the equations of motion are coupled, as it is shown by the equation referred to the k-th coordinate:

$$\ddot{p}(t)_k + 2\xi_k \omega_k \dot{p}(t)_k + \omega_k^2 p(t)_k + \theta_k\left(p(t)_1, p(t)_2, \ldots, p(t)_n\right) = U_{ki} F_i(t) \tag{7.1}$$

where p_k represents the principal coordinate, ξ_k the modal damping, ω_k the k-th natural frequency, $F_i(t)$ the force applied at position i in physical coordinates, U_{ki} the modal or basis vector and θ_k the non-linear component that couples the equations of motion.

In light of what it has been shown, whenever the excitation is high enough to induce a non-linear response in the system, one has to take into account modal interaction and internal resonances between different modes.

In some circumstances, especially in the case of resonant excitation applied to a weakly non-linear system, most of the energy is carried by a single resonant component, p_k,, the other components being negligible. This means that coupling in Equation (7.1)

vanishes and the system behaves as a SIMO (Single Input Multiple Output) system. In the specific case of the resonance tests conducted on the masonry bridge, the latter circumstance has been confirmed by experimental evidences, as it is shown in Figure 7.11. In fact, while at higher excitation levels the presence of internal resonances is evident (peculiarly in the 100 N excitation case), all resonance peaks are still related to the super-harmonics of the excited frequency, the coupling components being excluded.

For a non-linear characterisation purpose, one can neglect the interactions among principal responses and non-linearity may be ultimately studied through the following equation:

$$\ddot{p}(t)_k + 2\xi_k\omega_k\dot{p}(t)_k + \omega_k^2 p(t)_k + f_k\left(p(t)_k\right) = U_{ki}F_i(t) \tag{7.2}$$

where the non-linear modal component f_k is decoupled.

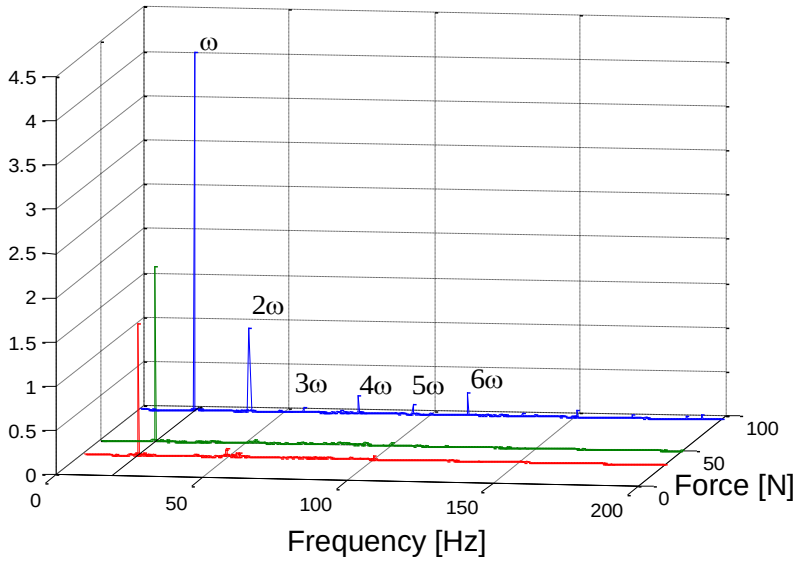

Figure 7.11 - Fast Fourier transforms of the bridge resonant response at the first natural frequency (18.9 Hz) using three different level of excitation.

7.4.2 Identification algorithm

The identification method assumes that the restoring force $f(p,\dot{p})$ can be described in a parametric form as:

$$\dot{f} = \hat{\dot{f}}\left(p, \dot{p}, f, \{par\}\right) \tag{7.3}$$

where the function $\hat{\dot{f}}(\cdot)$ depends on the state variables $p, \dot{p}$, on $f(\cdot)$ and on a model parameter vector {*par*}.

In order to extract instantaneous parameter estimates, it is possible to operate in the time domain e.g. (Lo & Hammond 1988, Wu & Smyth 2008) or in the time-frequency domain [6,9,10]. At any instant $\bar{t}$, the identification process leads to an associated optimal vector $\left\{par_{id}(\bar{t})\right\}$, which supplies instantaneous estimates of the parameters.

7.4.3 Non-linear identification from shaker tests

As previously stated, the bridge dynamic response has been treated as a series of SISO systems, using resonant excitation. In particular, the model proposed in equation (7.2) may be expressed in physical coordinates. For an excitation applied at position *i* and a response measured at position *j* one has:

$$\ddot{x}_{ki} + 2\xi_k \omega_k \dot{x}_{ki} + f\left(x_{ki}, \dot{x}_{ki}\right) = U_{kj} U_{ki} F_i(t) \tag{7.4}$$

The lower excitation levels are expected to show a predominance of the linear behaviour (Figure 7.11). Therefore, all the terms related to non-linear coefficients in equation (7.2) may be neglected. Then, these experimental data have been used in order to carry out a preliminary estimation of the linear characteristic of the system. In the consequent optimisation process, linear modal parameters, including a viscous equivalent damping, have been initialised to those available from a previous identification from ambient response signals (SSI algorithm) [1]. An initial estimate of the factor $U_{kj}U_{ki}$ has been conveniently obtained from the classical formula of viscous damping at resonance excitation.

The results of the instantaneous fitting are listed only for one single response point that is representative of the dynamic behaviour of the structure relative to the first mode. The instantaneous values show a good consistency respect to time, confirming that degrading effects were not occurring in the bridge and that the identification results are reliable.

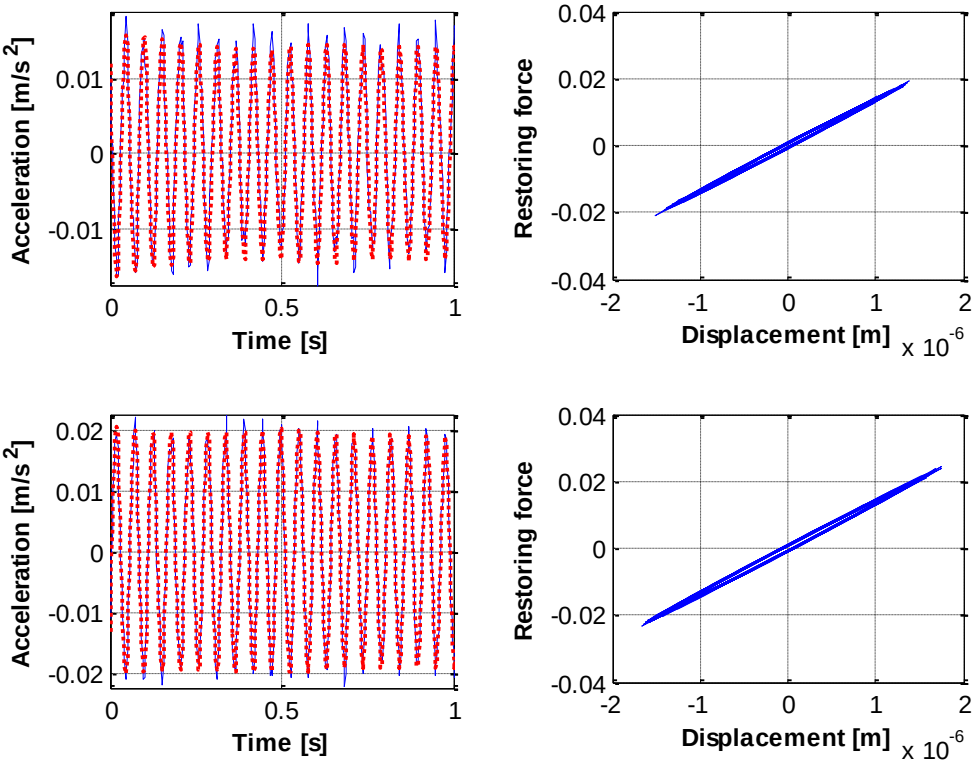

Figure 7.12 - Comparison between measured accelerations (blue-continuous line) with identified results (red-dashed line). Force-Displacement plot (experimental, right-side).

Figure 7.12 shows the comparison between experimental and identified data in terms of acceleration response to the first two excitation levels. As it is easily noticed, the behaviour of the system is substantially linear. The estimated parameters are reported in table 7.4.

Excitation Level	$U_{kj} \cdot U_{ki}$	ξ_k	ω_k
33 N	2.0e-5	0.026	117.60
66 N	1.7e-5	0.023	117.66

Table 7.4 - Identified linear parameters (average values).

For what concerns the highest excitation level, figure 7.13 depicts the phase plot of hysteretic force and displacement, showing a clear non-linear trend for higher amplitudes. In this case, the linear model would just lead to equivalent coefficients; therefore a Bouc-Wen model has been assumed to identify the system, so as to account for a more realistic rate-independent damping. Consequently the viscous, or rate-dependent,

damping term has been set to zero. It is noteworthy to remember that, in accordance with Equation (7.4), the identified hysteretic terms are affected by the factor $U_{kj} \cdot U_{ki}$.

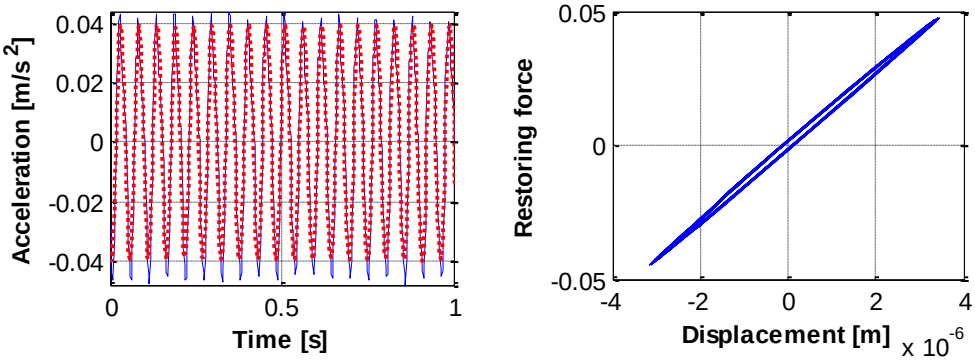

Figure 7.13 - Comparison between measured accelerations (blue-continuous line) with identified results (red-dashed line). Force-Displacement plot (experimental, right-side).

Figure 7.14 shows the instantaneous values of the Bouc-Wen coefficients. The γ parameter contribute resulted to be negligible; therefore it has not been reported. On the other hand, the β and n coefficients are almost constant, confirming the robustness of the method and the quality of the estimation.

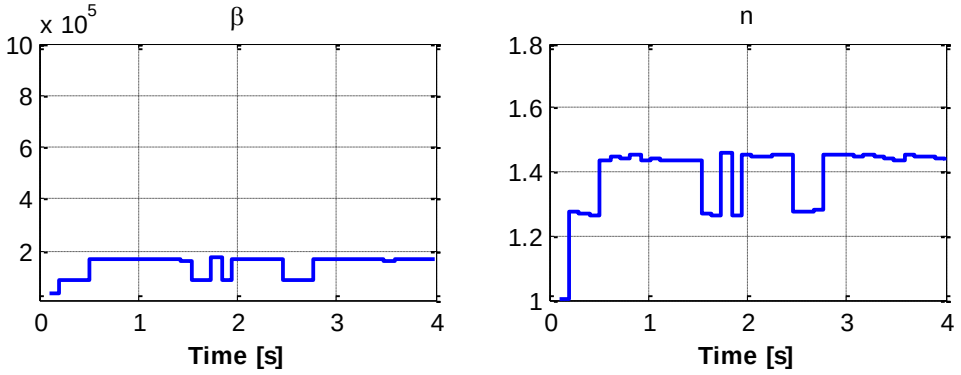

Figure 7.14 - Instantaneous identified hysteretic parameters: β left side, n right side.

Finally, a harmonic excitation characterised by higher amplitude (1000 N) has been applied to the identified hysteretic model. To this aim, a time averaging of the Bouc-Wen coefficients has been performed by using equation (7.4). The results obtained are shown in the diagram of figure 7.15, which exhibit clear hysteresis loops and infers an ideal behaviour at higher excitation levels.

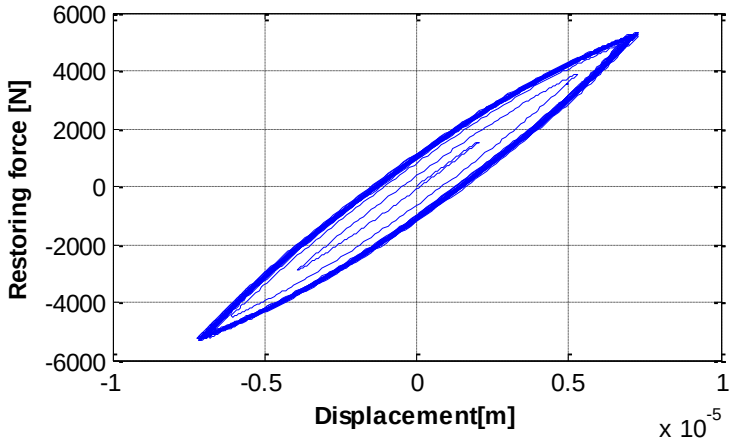

Figure 7.15 - Force - displacement hysteretic plot for high excitation amplitudes (β=1.83e5, γ=0, n=1.45).

7.4.4 Perspectives in non-linear model updating

The non-linear model identified may be used to update a FE model of the bridge. Therefore, a new FE model has been realised in ANSYS (see figure 7.16). This new model has also the new masses added at the top of the pier after the 1st campaign of dynamic investigation. The model has been realised using solid elements and spring elements to simulate the settlement application device. In perspective, this new model will be updated by using the data resulting from the non-linear identification. The prediction capability of the updated nonlinear model will be tested in future experimental campaigns.

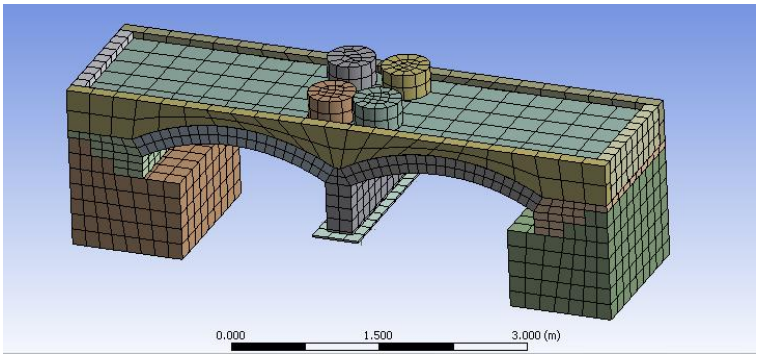

Figure 7.16 - Finite Element model realised in Ansys with the added mass to the bridge.

References

[1] Ruocci, G., (2010); *Application of the SHM methodologies to the protection of masonry arch bridges from scour*. Politecnico di Torino, PhD Thesis.

[2] Ruocci, G..D.L., Quattrone, A., Zanotti Fragonara, L., Ceravolo, R., De Stefano, A., (2011); *Experimental testing of a masonry arch bridge model subject to increasing level of damage*. Proceedings of 4th International Conference on Advances in Experimental Structural Engineering, Ispra.

[3] Ruocci, G., Quattrone, A., De Stefano, A., (2011); *Multi-domain feature selection aimed at the damage detection of historical bridges*. Journal of Physics. Conference Series, 305, pp. 1-10.

[4] Ruocci, G., Quattrone, A., Zanotti Fragonara, L., Ceravolo, R., De Stefano, A., (2011); *Instantaneous modal parameters estimation for real-time damage detection.* Proceedings of 8th International Conference on Structural Dynamics, Eurodyn, Leuven (Belgium).

[5] Choi, H.I., Williams, W.J., (1989); *Improved time-frequency representation of multicomponent signals using exponential kernels*. IEEE Trans. Acoust. Speech Signal Process, 37(6), pp. 862-871.

[6] Ceravolo, R., (2004); *Use of instantaneous estimators for the evaluation of structural damping*. J. of Sound and Vib., 274(1-2), pp. 385-401.

[7] Bellizzi, S., Bouc, R., (1999); *Analysis of multi-degree of freedom strongly non-linear mechanical systems with random input Part I: Non-linear modes and stochastic averaging*. Probabilistic Engineering Mechanics, 14, pp. 229-244.

[8] Spottswood, S.M., Allemang, R.J., (2006); *Identification of nonlinear parameters for reduced order models*. Journal of Sound and Vibration, 295, pp. 226-245.

[9] Ceravolo, R., Demarie, G.V., Erlicher, S., (2010); *Instantaneous identification of degrading hysteretic oscillators under earthquake excitation*. Struct. Health Monitor., 9(5), pp. 447-464.

[10] Ceravolo, R., Zanotti Fragonara, L., Erlicher, S., Bursi, O.S., (2011); *Parametric identification of damaged dynamic systems with hysteresis and slip*. Journal of Physics: Conference Series.

[11] Ceravolo, R., De Stefano, A., Quattrone, A., Zanotti Fragonara, L., Ruocci, G., (2011); *Using non-linear identification from shaker tests for structural reliability assessment*. Proceedings of EVACES 2011, Experimental Vibration Analysis for Civil Engineering Structures, Varenna, pp. 801-808.